# Full-Wave Analysis of Coplanar Waveguide Discontinuities Using the Frequency Domain TLM Method

Hang Jin, *Member, IEEE,* and Rüdiger Vahldieck, *Senior Member, IEEE*

***Abstract*—This paper presents a full-wave analysis of a variety of coplanar waveguide discontinuities using the frequency domain TLM method. The finite metallization thickness is taken into account as well as metal losses and the interaction of fundamental and higher order modes between cascaded discontinuities. Numerical results are presented for the frequency-dependent $s$-parameters of transitions between CPW and slotline, CPW and microstrip line and CPW-microstrip overlap transition. The effect of interactions between the CPW discontinuities and the CPW airbridges is also investigated.**

## I. Introduction

COPLANAR WAVEGUIDES (CPW) are widely used in monolithic microwave integrated circuits (MMICs) and miniaturized MICs on alumina substrate. The knowledge of transmission line parameters like propagation constant and characteristic impedance alone is not sufficient any longer to design CPW circuits because the high circuit density of active and passive devices may lead to electromagnetic interference between circuit parts. Instead the scattering parameters of hybrid modes at discontinuities is important as well as the interaction between fundamental and higher order modes between discontinuities. While many papers have been published dealing with propagation constant, characteristic impedance, and losses on straight line CPWs i.e., [1]–[8], there are only few contributions characterizing CPW discontinuities, i.e., [9]–[11], [19]. The most general papers so far are by Huang and Itoh [12] and by Jin and Vahldieck [13]. In [12], a combination of the spectral domain approach and mode matching method has been utilized to analyze $s$-parameters for CPW to slotline transitions including the effect of finite metallization thickness. In [13], $s$-parameters for CPW discontinuities and airbridges including metal thickness ad losses have been analyzed using the frequency-domain TLM method. Both papers have shown that the finite metallization thickness should be taken into account as well as the mode interaction between cascaded discontinuities.

Since MMICs are typically composed of a variety of different types of transmission lines, low loss connection between the different propagation media, i.e., CPW to slotline or CPW to microstrip, is of considerable concern in the design of components like balanced mixers, multipliers, switches etc. In this paper, the frequency-domain TLM (FDTLM) [15] method is used to investigate a variety of CPW discontinuities including the overlay transition between a CPW and a microstrip line and to characterize the effects of changes in the structural dimensions. The close proximity of a CPW discontinuity to an airbridge as well as a discontinuity in an airbridge bridging the center conductor instead of the groundplane, is also investigated.

The FDTLM method is a new and very powerful 3-D full-wave analysis technique which has been described by the authors in detail in [14], [15]. Therefore only a brief description of this technique is given in Section II. Although dielectric and metallic losses as well as isotropic and anisotropic dielectric is automatically taken into account in this approach, the analysis presented in this paper is only focused on the $s$-parameters of discontinuities versus circuit dimensions and frequency. The interaction of fundamental and higher order hybrid modes at discontinuities and between cascaded discontinuities is included in the algorithm.

## II. Theory

In the FDTLM method, the space to be analyzed is discretized by a transmission line network, as in the conventional time domain TLM (TDTLM) method. However, instead of exciting the network with a single impulse, the excitation used in the FDTLM is an impulse train with its magnitude sinusoidally modulated so that the magnitudes of the impulses vary with time as $e^{j\omega N\Delta t}$, where $\omega$ is the modulation frequency, $N$ the time step, and $\Delta t$ the time interval between impulses. This impulse train is assumed to be injected into the TLM network at the time $t = -\infty$. At present time $t$, a steady-state impulse distribution is observed and the magnitudes of subsequent impulses at any node are related by a factor of $e^{j\omega\Delta t}$. Therefore, if the magnitude of the impulse at a particular reference time is known, the magnitude of the impulse at any other time step can be readily found by multiplying with $e^{j\omega\Delta N\Delta t}$, where $\Delta N\Delta t$ is the total time interval between the reference time step and the time when the observation takes place. Thus, the time iteration procedure necessary in the conventional TDTLM method is no longer needed in the FDTLM method. For the actual realization of the computer algorithm no impulse excitation is required. The assumption of an excitation as described before is just to simplify the

Manuscript received September 20, 1993; revised February 3, 1993.

The authors are with the Laboratory for Lightwave Electronics, Microwaves, and Communications, Department of Electrical and Computer Engineering, University of Victoria, Victoria, B.C., Canada.

IEEE Log Number 9211864.

algorithm and to provide the transition between the TDTLM and the FDTLM [15]. As shown in [15], the FDTLM algorithm operates within one time step at an arbitrary time instance. Therefore, in the computation, the common time-dependent factor $e^{j\omega N\Delta t}$ can be omitted. This is an analogy to other frequency-domain methods where a sinusoidal excitation is assumed and the steady-state response is simply the product of a space-dependent quantity and the time factor $e^{j\omega t}$, which is also omitted for practical computations. The only difference is that, for ordinary frequency-domain methods, the time-dependent factor is a continuous function of time $(e^{j\omega t})$, while for the FDTLM it is a discrete function $(e^{j\omega N\Delta t})$ of time because the TLM network always discretizes space and time simultaneously regardless of the kind of excitation. This leads to a slightly different representation for Maxwell's equation in the FDTLM where the time axis is discretized on the right-hand side of the equation as followed:

$$\nabla \times Ee^{j\omega N\Delta t} = -\mu \frac{e^{j\omega(N+1)\Delta t} - e^{j\omega N\Delta t}}{\Delta t} H$$
$$\nabla \times He^{j\omega N\Delta t} = \varepsilon \frac{e^{j\omega(N+1)\Delta t} - e^{j\omega N\Delta t}}{\Delta t} E. \quad (1)$$

By omitting the common factor $e^{j\omega N\Delta t}$ on both sides of (1) we yield

$$\nabla \times E = -j\omega\mu \frac{e^{j\omega\Delta t} - 1}{j\omega\Delta t} H$$
$$\nabla \times H = j\omega\varepsilon \frac{e^{j\omega\Delta t} - 1}{j\omega\Delta t} E. \quad (2)$$

Comparing (2) with the time-harmonic representation of Maxwell's equations [17], we find that there is an additional factor on the right-hand side of (2). This additional factor approaches unity if $\omega\Delta t$ approaches zero. It is obvious from (2) that the additional factor from the time discretization leads to the dispersion problem in the TLM network. In the FDTLM, this dispersion problem can be easily eliminated by modifying the material permittivity and permeability in the following way:

$$\nabla \times E = -\bar{\mu} \frac{\partial H}{\partial t}$$
$$\nabla \times H = \bar{\varepsilon} \frac{\partial E}{\partial t} \quad (3)$$

with $\bar{\mu} = \mu(j\omega\Delta t)/(e^{j\omega\Delta t}-1)$ and $\bar{\varepsilon} = \varepsilon(j\omega\Delta t)/(e^{j\omega\Delta t}-1)$. Hence, after the time axis is discretized, (3) becomes identical to the time harmonic representation of Maxwell's equations.

The algorithm of the FDTLM is based on the concept of the *intrinsic scattering matrix* $m$, which is, in general, defined as the coefficient matrix relating the reflected and incident impulses at the exterior branches of a TLM network. An explicit expression for the intrinsic scattering matrix $m$ has been given in [15] in terms of the scattering matrix $S$ and connection matrix $C$ of the TLM network. Once the intrinsic scattering matrix is known, all the properties of the structures can be computed through matrix operations. In the following, a brief description of the algorithm of the FDTLM will be given for the case of a two-port discontinuity problem, which consists of a discontinuity region and two attached semi-infinity waveguides as input and output ports (Fig. 1). First, we find the intrinsic scattering matrices for the discontinuity region and the two attached semi-infinity waveguides. They are denoted $m, R_1$, and $R_2$, respectively. The incident and reflected impulses at the interfaces to the discontinuity region and the attached waveguides are related as follows:

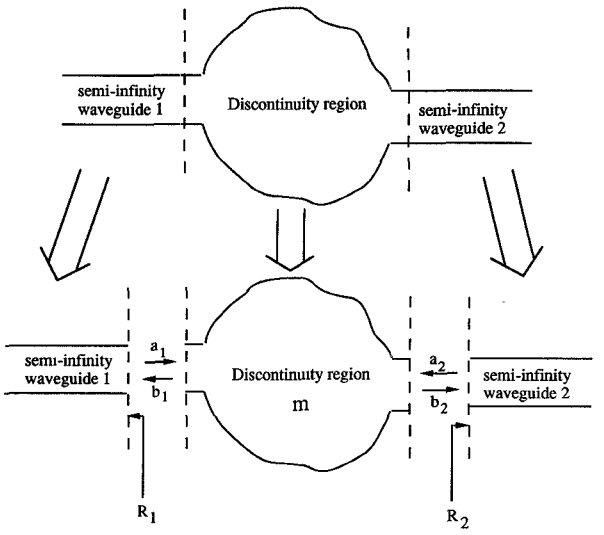


Fig. 1. Two-port discontinuity problem consisting of a discontinuity region and two attached semi-infinity waveguides.

$$\begin{pmatrix} b_1 \\ b_2 \end{pmatrix} = m \cdot \begin{pmatrix} a_1 \\ a_2 \end{pmatrix} = \begin{pmatrix} m_{11} & m_{12} \\ m_{21} & m_{22} \end{pmatrix} \cdot \begin{pmatrix} a_1 \\ a_2 \end{pmatrix} \quad (4)$$

where $a_1, b_1$ are the incident and reflected impulse vectors at the interface of waveguide one and the discontinuity region; while $a_2, b_2$ are the incident and reflected impulse vectors at the interface of waveguide two and the discontinuity region (each element of these vectors corresponds to one branch of the network). The excitation of the system, $a_{10}$ and $b_{10}$, which is obtained from a 2-D analysis [15], is incident at the interface between waveguide one and the discontinuity region. It should be noted that vector $a_{10}$ and $b_{10}$ describe the field distribution over the cross-section of waveguide one. The reflected waves, $a_1', b_1'$, at waveguide one are then given by

$$a_1' = R_1 \cdot b_1' \quad (5)$$
$$b_1' = (1 - R_2' \cdot R_1)^{-1} \cdot (R_2' - R_1) \cdot a_{10} \quad (6)$$

where $R_2'$

$$R_2' = m_{11} + m_{12} \cdot R_2 \cdot T' \quad (7)$$
$$T' = (1 - m_{22} \cdot R_2)^{-1} \cdot m_{21} \quad (8)$$

$a_2, b_2$ at waveguide two are obtained from

$$a_2 = R_2 \cdot b_2 \quad (9)$$
$$b_2 = T' \cdot a_1 = T' \cdot (R_1 \cdot b_1' + a_{10}). \quad (10)$$

From (4)–(10), the corresponding $s$-parameters can be obtained [15].

## III. Numerical Results and Discussions

A variety of structures have been analyzed and the results from the FDTLM analysis and existing data have been compared in order to validate the accuracy of the method. Since field components for the different modes can be separated in the FDTLM method, the reference plane for the $s$-parameter calculation may be located right in the discontinuity interface. This is an important advantage of this new method because it allows to reduce the volume of the space to be discretized to the discontinuity plane. There is no need to perform the Fourier transform on the output wave. Also, the dispersion effect resulting from the time discretization in the TLM network can be easily compensated as discussed before. Thus, truncation and velocity errors known from the TDTLM no longer exist in the FDTLM. Furthermore, extensive calculations show that the FDTLM is quite robust with respect to the mesh size. For example, a rectangular waveguide only needs 5 nodes for the $a$-dimension and 2 nodes for the $b$-dimension. The numerical result of the propagation constant with this mesh layout is within 1% from the exact solution. In addition, the ratio of mesh sizes of adjacent nodes may change in a wide range from 0.001 to 1000 without causing any numerical problems. Such a large ratio for the mesh size is often required in cases where structures have widely varying dimensions. In the calculation, the coarseness error is reduced by using a nonuniform mesh layout to provide higher resolution in the non-uniform field region. To test the accuracy of the results, a structure is usually analyzed twice with two different mesh layouts. If the discrepancy between the two results is within 1%, the results are considered accurate. The CPU-time required to compute the following structures is on the average between 2–5 minutes on a SUN SPARC STATION 2.

In the following analysis, the metallization thickness is always considered and assumed to be $3\mu$m. Also, all structures are placed in a metallic enclosure which is small enough as to not support waveguide modes but still large enough as to not influence the CPW (slotline or microstrip mode) mode. The $s$-parameters are all normalized to the characteristic impedance of the connecting lines (which are not necessarily 50Ω). Fig. 2 shows the frequency-dependent $s$-parameters for a finline to CPW transition considering a quarter wave transformer section for better matching of the finline mode, which is the receive mode in a front-end application [19]. A significantly improved match at about 25 GHz is obtained. At this frequency the propagation constant of the intermediate slotline is $\beta = 1.1$ ($\text{mm}^{-1}$) and the quarter wavelength is about $\lambda g = 2\pi/4\beta = 1.43$, which is very close to the physical length of the added section ($d_1 = 1.5$ mm). Varying the gap $g$ between the finline and the CPW, it was found that the results for two different gaps ($g = 0.1$ mm and $g = 3.0$ mm) are almost identical, indicating that this kind of transition is not sensitive with respect to the distance between the two transmission lines.

Fig. 3 shows a CPW to microstrip transition with an odd mode excitation. The walls of the metallic enclosure are $2 \times S2 + W1$, which means the CPW groundplane and the backmetallization (the latter one is the groundplane for the microstrip line) are on the same potential. Due to the additional

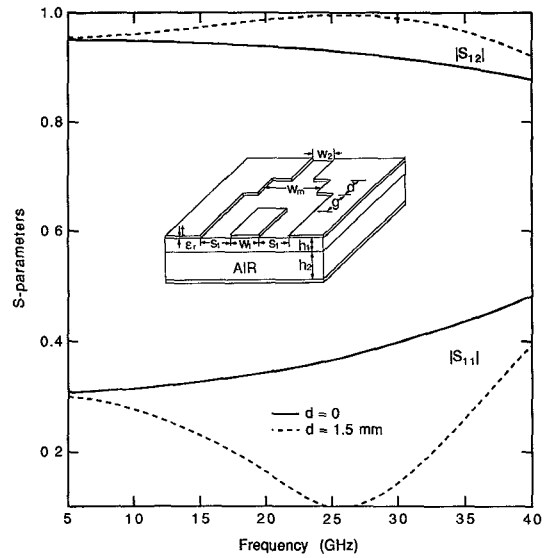


Fig. 2. Frequency-dependent $S$-parameters of a cascaded CPW-finline transition ($w_1 = 0.2$ mm, $s_1 = 0.6$ mm, $w_2 = 0.4$ mm, $w_m = 1.0$ mm, $h_1 = 0.254$ mm, $h_2 = 0.4$ mm, $t = 0.003$ mm, $\varepsilon_r = 9.6$, and the metallization $\sigma = 10000$ s/mm).

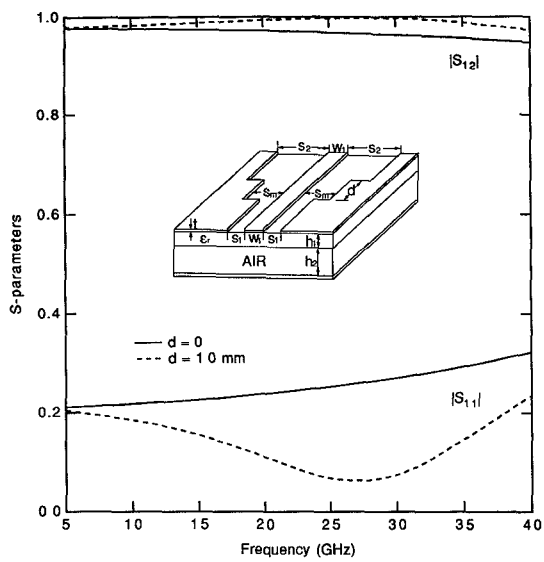


Fig. 3. Frequency-dependent $S$-parameters of a CPW to microstrip transition ($w_1 = 0.2$ mm, $s_1 = 0.1$ mm, $s_m = 0.2$ mm, $s_2 = 5.0$ mm, $h_1 = 0.254$ mm, $h_2 = 0.2$ mm, $t = 0.003$ mm, $\varepsilon_r = 9.6$, and the metallization $\sigma = 10000$ s/mm).

substrate layer (air $\varepsilon_r = 1.0$) between the back metallization and the alumina substrate ($\varepsilon_r = 9.6$) [18], there are no higher order modes up to 40 GHz. As expected, the reflection coefficient increases with frequency because the transition behaves like a transmission line junction with a parasitic shunt capacitor. The characteristic impedances are 54Ω for the CPW and 97Ω for the microstrip. Also, here the reflection coefficient can be reduced by introducing a quarter wavelength (CPW) transformer between both transmission lines. The lowest value for $S_{11}$ in Fig. 4 occurs at about 28 GHz which corresponds to $\beta = 1.5$ ($\text{mm}^{-1}$) or a quarter wavelength $\lambda g \sim 1.05$ mm, which is approximately the physical length of the intermediate section ($d = 1$ mm).

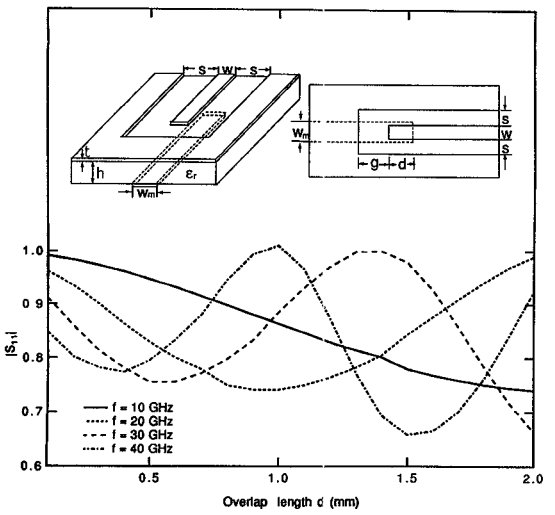


Fig. 4. $S$-parameter versus overlap length $d$ of the CPW to microstrip overlap transition as shown in Fig. 5. ($w$ = 0.2 mm, $s$ = 0.1 mm, $w_m$ = 0.2 mm, $h$ = 0.254 mm, $g$ = 0.5 mm, $\varepsilon_r$ = 9.6, and the metallization $\sigma$ = 10000 s/mm).

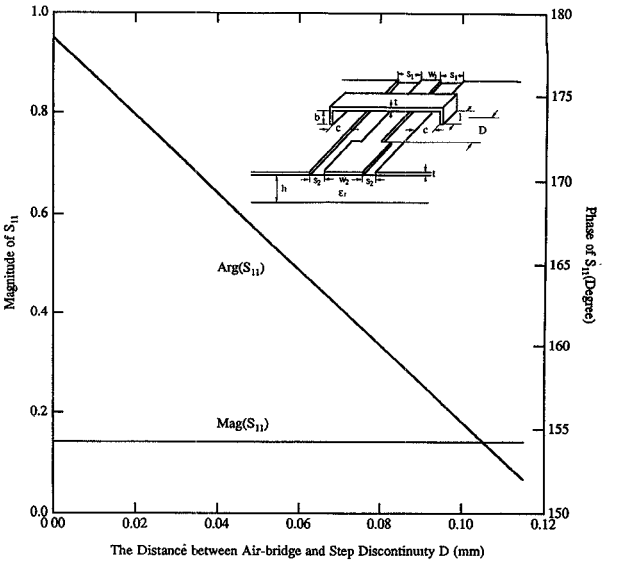


Fig. 5. Cascading a CPW discontinuity and an airbridge. Frequency = 40 GHz, $w_1$ = 12$\mu$m, $w_2$ = 20$\mu$m, $s_1$ = 12$\mu$m, $s_2$ = 8$\mu$m, 1 = 30$\mu$m, $b$ = 3$\mu$m, $h$ = 100$\mu$m, $t$ = 3$\mu$m, $\varepsilon_r$ = 12.9, and the metallization $\sigma$ = 10000 s/mm).

An overlay transition between a microstrip and a CPW is shown in Fig. 4. This transition provides electromagnetic coupling between two transmission lines of 54Ω characteristic impedance. As expected, the coupling between both transmission media increases with overlap area and at the same time the $s$-parameters become more frequency dependent.

The interaction effect between an airbridge and a discontinuity in the center conductor of the CPW is shown in Fig. 5. The characteristic impedance of the CPW is 45 and 50Ω, respectively. As illustrated in the figure, the actual location of the airbridge with respect to the discontinuity has virtually no effect on the $s$-parameters. Similarly Fig. 6 demonstrates the influence of an airbridge in which the center conductor is bridged across the groundplane. The characteristic impedance on either side of the airbridge is 70 and 50Ω, respectively. The step between both impedances takes place within the airbridge. Also, here the location of this step has little impact on the overall $s$-parameters.

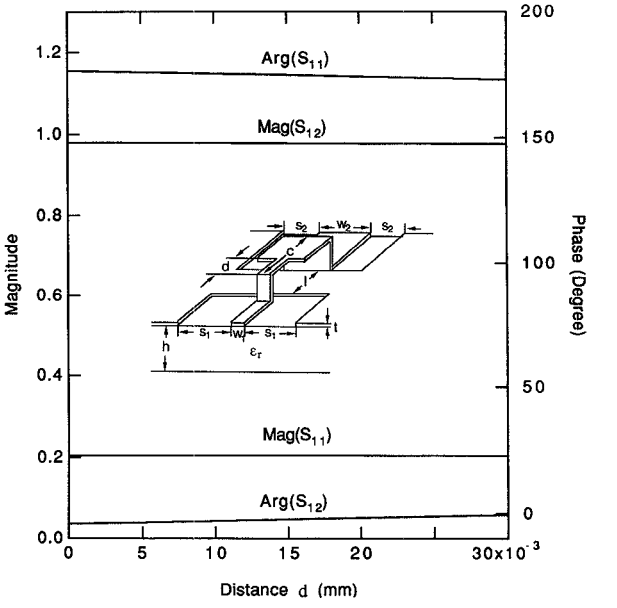


Fig. 6. Airbridge discontinuity connecting a 70Ω and 50Ω CPW. Frequency = 40 GHz ($w_1$ = 10$\mu$m, $w_2$ = 21$\mu$m, $s_1$ = 12.5$\mu$m, $s_2$ = 7$\mu$m, 1 = 30$\mu$m, $c$ = 45$\mu$m, $b$ = 3$\mu$m, $h$ = 100$\mu$m, $t$ = 3$\mu$m, $\varepsilon_r$ = 9.8, and the metallization $\sigma$ = 10000 s/mm).

## IV. Conclusions

This paper has introduced a rigorous analysis of a variety of CPW discontinuities using the frequency-domain TLM method. Numerical results of frequency-dependent $s$-parameters have been presented which include the effect of finite thickness and conductivity of metallization as well as mode interaction between cascaded discontinuities. Electromagnetic coupling between microstrip and CPW overlay couples and the proximity effects of CPW discontinuities and air-bridges have been investigated. Single-step $\lambda g/4$-wave transformers have been designed to lower the reflection coefficient between a CPW to microstrip and slotline to CPW transition.

## References

[1] M. Riaziat, R. Majidi-Ahy, and I. J. Feng, "Propagation modes and dispersion characteristics of coplanar waveguides," *IEEE Trans. Microwave Theory Tech.*, vol. 38, pp. 245–251, Mar. 1990.

[2] R. W. Jackson, "Consideration in the use of coplanar waveguide for millimeter-wave integrated circuits," *IEEE Trans. Microwave Theory Tech.*, vol. 34, pp. 1450–1456, Dec. 1986.

[3] T. Kitazawa and Y. Hayashi, "Quasistatic and hybrid-mode analysis of shielded coplanar waveguide with thick metal coating," *Proc. IEE*, vol. 134, pt. H, pp. 321–323, 1987.

[4] H. J. Finlay, R. H. Jansen, J. A. Jenkins, and I. G. Eddison, "Accurate characterization and modelling of transmission lines for GaAs MMICs," *IEEE Trans. Microwave Theory Tech.*, vol. 36, pp. 961–967, June 1988.

[5] W. Heinrich, "Full-wave analysis of conductor losses on MMIC transmission lines," *IEEE Trans. Microwave Theory Tech.,* vol. 38, pp. 1468–1472, Oct. 1990.
[6] S. S. Bedair and I. Wolff, "Fast, accurate and simple approximate analytic formulas for calculating the parameters of supported coplanar waveguides for MMICs," *IEEE Trans. Microwave Theory Tech.,* vol. 40, pp. 41–48, Jan. 1992.
[7] R. Sorrentino, G. Leuzzi, and A. Silbermann, "Characteristics of metal-insulator-semiconductor coplanar waveguides for monolithic microwave circuits," *IEEE Trans. Microwave Theory Tech.,* vol. 32, pp. 410–415, 1984.
[8] G. Ghione and C. Naldi, "Coplanar waveguides for MMIC applications: Effect of upper shielding, conductor backing, finite-extend groundplanes, and line to line coupling," *IEEE Trans. Microwave Theory Tech.,* vol. 35, pp. 260–267, 1987.
[9] M. Naghed and I. Wolff, "Equivalent capacitances of coplanar waveguide discontinuities and interdigital capacitors using 3-D finite difference method," *IEEE Trans. Microwave Theory Tech.,* vol. 38, pp. 1808–1815, Dec. 1990.
[10] J. S. Mclean and T. Itoh, "Fullwave analysis of the radiative properties of short-circuit discontinuities in modified coplanar stripline," presented at the 1992 IEEE Int. Microwave Symp. Dig., pp. 203–206.
[11] R. H. Jansen, "A full-wave electromagnetic model of cylindrical and conical via hole ground for use in interactive MIC/MMIC design," presented at the 1992 IEEE Int. Microwave Symp. Dig., pp. 1233–1236.
[12] T. W. Huang and T. Itoh, "Full-wave analysis of cascaded junction discontinuities of shielded coplanar type transmission line considering the finite metallization thickness effect," presented at the 1992 IEEE Int. Microwave Symp. Dig., pp. 995–998.
[13] H. Jin and R. Vahldieck, "Calculation of frequency-dependent $S$-parameter of CPW air bridges considering finite metallization thickness and conductivity," presented at the 1992 IEEE Int. Microwave Symp. Dig., pp. 207–210.
[14] ——, "A frequency domain TLM method," presented at the 1992 IEEE Int. Microwave Symp. Dig., pp. 775–778.
[15] ——, "The frequency-domain transmission line matrix method—A new concept," *IEEE Trans. Microwave Theory Tech.,* Dec. 1992, (to be published).
[16] W. J. R. Hoefer, "The transmission line matrix method," *IEEE Trans. Microwave Theory Tech.,* vol. 33, pp. 882–893, Oct. 1985.
[17] S. Ramo, J. R. Whinnery, and T. V. Duzer, *Fields and Waves in Communication Electronics. (2nd ed.)* New York: Wiley, 1984.
[18] K. Wu and R. Vahldieck, "Rigorous analysis of the characteristic impedance in conductor-backed miniature coplanar waveguide considering multiple layers of lossy and finite thickness metal," presented at the 1992 IEEE Int. Microwave Symp. Dig., pp. 987–990.
[19] C. Sinclair and S. Nightingale, "An equivalent model for the coplanar waveguide step discontinuity," presented at the 1992 IEEE Int. Microwave Symp. Dig., pp. 1461–1464.

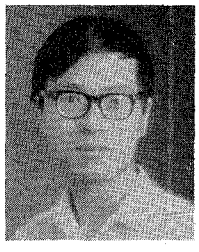

**Hang Jin,** (M'91) was born in Jiangsu, China, on September 27, 1960. He received the B.Sc. degree in electrical engineering from the University of Science and Technology of China (USTC), Hefei, China, in 1982 and M. Eng. and D. Eng. degrees in electrical engineering from the University of Electronics Science and Technology of China, Chengdu, China, in 1984 and 1987, respectively.

Dr. Jin joined the Faculty at the University of Electronics Science and Technology of China in 1987 where he conducted research in the areas of electromagnetic scattering, radar absorbing material, and millimeter wave techniques. From 1989–1990, he was a postdoctoral fellow at the National Optics Institute, Quebec City, PQ, Canada.

Since October 1990, he has been a Research Associate at the University of Victoria, Victoria, BC, Canada. His current research areas include numerical methods for 3-D electromagnetic field problems, CAD of microwave/millimeter wave integrated (monolithic) circuits, and planar and quasi-planar components for MMIC and MHMIC applications

**Rüdiger Vahldieck,** (M'85–SM'86) received the Dipl.-Ing. and the Dr.-Ing. degrees in electrical engineering from the University of Bremen, West Germany, in 1980 and 1983, respectively.

From 1984 to 1986 he was a Research Associate at the University of Ottawa, Canada. In 1986 he joined the University of Victoria, British Columbia, Canada, where he is now a Full-Professor in the Department of Electrical and Computer Engineering. During Fall and Spring 1992–'93 he was a visiting scientist at the "Ferninand-Braun-Institute für Hochfrequenztechnik" in Berlin, Germany. His research interests include numerical methods to model electromagnetic fields for computer-aided design of microwave, millimeter wave and opto-electronic integrated circuits. He is interested in design aspects of passive and active planar and quasi-planar components for MMIC and MHMIC applications. Recently he has been involved in research on subcarrier multiplexed lightwave systems. The emphasis of this work is on broad bandwidth electro-optic modulators and on coherent detection systems in fiber-optic communication links.

Dr. Vahldieck, together with three coauthors, received the outstanding publication award of the Institution of Electronic and Radio Engineers in 1983. He is on the Editorial Board of the IEEE TRANSACTIONS ON MICROWAVE THEORY AND TECHNIQUES and has published more than 100 technical papers mainly in the field of microewave CAD.